Article

Thiols Passivate Recombination Centers in Colloidal Quantum Dots Leading to Enhanced Photovoltaic Device Efficiency

D. Aaron R. Barkhouse, Andras G. Pattantyus-Abraham, Larissa Levina, and Edward H. Sargent

ACS Nano, **2008**, 2 (11), 2356-2362 • Publication Date (Web): 06 November 2008

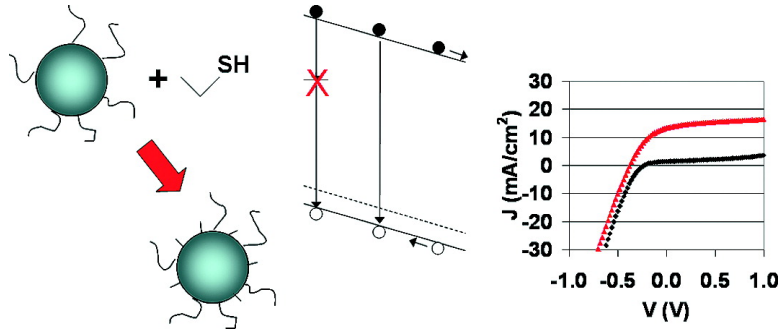

More About This Article

Additional resources and features associated with this article are available within the HTML version:

- Supporting Information
- Access to high resolution figures
- Links to articles and content related to this article
- Copyright permission to reproduce figures and/or text from this article

View the Full Text HTML

ARTICLE

Thiols Passivate Recombination Centers in Colloidal Quantum Dots Leading to Enhanced Photovoltaic Device Efficiency

D. Aaron R. Barkhouse, Andras G. Pattantyus-Abraham, Larissa Levina, and Edward H. Sargent*

Edward S. Rogers Department of Electrical and Computer Engineering, University of Toronto, 10 King's College Road, Toronto, Ontario M5S 3G4, Canada

ABSTRACT The use of thiol-terminated ligands has recently been reported to enhance 10-fold the power conversion efficiency (PCE) of colloidal quantum dot (CQD) photovoltaic (PV) devices. We find herein that, in a representative amine-capped PbS colloidal quantum dot materials system, improved mobility following thiol treatment accounts for only a 1.4-fold increase in PCE. We then proceed to investigate the origins of the remainder of the quadrupling in PCE following thiol treatment. We find through measurements of photoluminescence quantum efficiency that exposure to thiols dramatically enhances photoluminescence in colloidal quantum dot films. The same molecules increase open-circuit voltage (V_{oc}) from 0.28 to 0.43 V. Combined, these findings suggest that mid-gap states, which serve as recombination centers (lowering external quantum efficiency (EQE)) and metal—semiconductor junction interface states (lowering V_{oc}), are substantially passivated using thiols. Through exposure to thiols, we improve EQE from 5 to 22% and, combined with the improvement in V_{oc}, improve power conversion efficiency to 2.6% under 76 mW/cm^2 at 1 μm wavelength. These findings are consistent with recent reports in photoconductive PbS CQD photodetectors that thiol exposure substantially removes deep (0.3 eV) electron traps, leaving only shallow (0.1 eV) traps.

KEYWORDS: lead sulfide · quantum dot · solution-processed · photovoltaic · ethanethiol · passivation · recombination

Solution-processed solar cells are of great technological interest due to their low-cost fabrication and their potential to provide efficient conversion of solar energy.[1,2] Organic solar cells made by solution processing have already exhibited 6.5% AM1.5 solar power conversion efficiency,[3] but under-utilize the 45% of terrestrial solar radiation that lies in the infrared. Infrared (IR) band gap quantum dots such as PbS[4−12] and PbSe[13−15] offer an attractive means of capturing energy in this portion of the spectrum due to the ease of tuning their band gap by quantum confinement.[16,17] The recent report of PbS CQD PV devices with 4.2% monochromatic PCE under 975 nm monochromatic illumination shows that the goal of efficient harvesting of near-IR radiation is seeing rapid progress.[9]

Many recent advances in quantum dot PV film properties and device performance have been made using treatments that involve thiols.[10,11,13,15] A layer-by-layer dipcoating process, starting with a porous ITO substrate and alternating PbS nanocrystal deposition and ethanedithiol (EDT) treatment, led to PV devices with 1.3% PCE under 12 mW/cm^2 illumination at 975 nm.[10] Highly conductive and uniform films of PbSe nanocrystals have been produced using a similar layer-by-layer dipcoating method, this time on a planar ITO substrate, with EDT as the insolubilizing agent.[15] More recently, PbSe Schottky PV devices produced by solid-state treatment of oleic-acid-capped nanocrystals with benzenedithiol reached 3.6% PCE under monochromatic 12 mW/cm^2 near-IR illumination.[13] The latter report also showed a tremendous increase in stability of device efficiency, both in an inert ambient and in room air, as a result of effective and robust passivation attributed to the thiol functional group.

In each of these reports, the beneficial effects of thiol treatment on PV device performance have been substantially attributed to a shortening of interdot distance,[10,11,13,15] improved cross-linking of dots,[10,11,13] and improved surface passivation.[13] In the related field of photoconductive photodetectors based on colloidal quantum dots,[18,19] thiol treatments have improved mobility but also reduced lag by repassivating deep trap centers.[20,21]

Here, we investigate a new route to producing PbS CQD PV devices that represents a simpler, faster route to device fabrication than the best previous report.[9] In the course of our study, we found that, in addition to improving the mobility in films of PbS quantum dots, treatment using ethanethiol leads to an improvement in carrier collection far greater than that expected from transport considerations alone. We use a combination

*Address correspondence to ted.sargent@utoronto.ca.

Received for review July 25, 2008 and accepted October 20, 2008.

Published online November 6, 2008. 10.1021/nn800471c CCC: $40.75

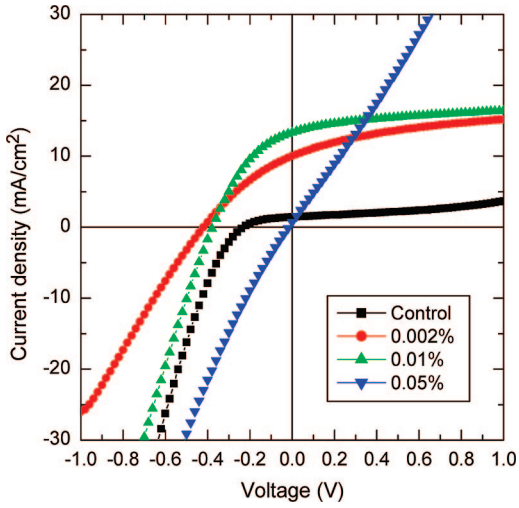

Figure 1. Current−voltage characteristics of devices treated with various concentrations of ethanethiol.

of luminescence spectroscopy and device optoelectronic behavior to elucidate the role of thiol-mediated recombination-center passivation as a major contributor to thiols' beneficial effects on performance.

RESULTS AND DISCUSSION

Investigation of EQE and Open-Circuit Voltage in Controls and in Thiol-Treated Photovoltaic Devices. Schottky PV devices were made by spin-coating a layer of butylamine-exchanged nanocrystals (see Methods section for details) onto precleaned ITO substrates. To study the effect of ethanethiol treatment on device performance, nanocrystal films were wetted with a dilute solution of ethanethiol in acetonitrile for 30 s prior to top-contact (Al/Ag) deposition.

Figure 1 shows current−voltage ($I-V$) curves of Schottky PV devices, treated with various concentrations of ethanethiol in acetonitrile, under 76 mW/cm^2 monochromatic illumination at 975 nm. It is clear that ethanethiol treatment results in an increase in both short-circuit current (J_{sc}) and V_{oc} for treatment concentrations up to 0.02%. Fourier transform infrared (FTIR) spectra indicated less than 10% reduction in oleic acid content following ethanethiol treatment for thiol concentrations up to 0.02% (see Figure S1 in the Supporting Information). Treatment with the optimum thiol concentration (0.01%) resulted in a PCE of 2.6% under 76 mW/cm^2 illumination at 975 nm, compared to 0.19% for the untreated controls. The EQE improved from 5 to 22%, while the V_{oc} increased from 0.28 to 0.43 V. It should be noted that, while these PCE values are modestly lower than the best reported value for a PbS CQD PV device,[9] the present investigation concerns the development of a much more rapid fabrication procedure (enabled by using the 2 h ligand exchange process described in the Methods section, as opposed to the 3 day procedure described previously[9]). This enables investigation of physical mechanisms and trends underlying the enhancements provided by thiol exposure compared to controls.

Treating with concentrations higher than 0.02% frequently led to a dramatic reduction in both V_{oc} and J_{sc}, consistent with a low shunt resistance in devices. Scanning electron microscope (SEM) images of these overtreated devices (Figure 2) show that, relative to a device treated with an ethanethiol concentration of 0.02%, overtreated films exhibit the formation of cracks. It is believed that overtreatment leads to stress in the film which is relieved by the formation of these cracks. These cracks may become filled with Al during top contact deposition, leading to shorting in the device.

Measurement of Electron and Hole Mobility Increase Resulting from Thiol Treatments. Thiols have been shown to affect significantly the electrical properties of nanocrystal films. To evaluate the role of this effect in our system, we measured the effect of ethanethiol treatment on the majority carrier (hole) and minority carrier (electron) mobilities using the carrier extraction by linearly increasing voltage (CELIV)[22] and time-of-flight (TOF) techniques, respectively. Figure 3 shows the hole mobility as a function of ethanethiol treatment concentration. Relative to untreated control devices, the mobility increases up to 4-fold for the highest treatment concentration, from 1.1 $\times$ 10^{-4} to 4.3 $\times$ 10^{-4} cm^2/Vs. This increase in mobility may be attributed to a decrease in interparticle spacing or a decrease in trap state density or depth in the treated devices. The electron mobility of control and ethanethiol-treated devices were found to be (2.6 $\pm$ 0.5) $\times$ 10^{-4} and (1.0 $\pm$ 0.4) $\times$ 10^{-4} cm^2/Vs, respectively. While it is possible that the electron mobility could be reduced by the introduction of electron trap states following thiol treatment, we feel that the time-of-flight mobility measurements are best treated as a rough gauge of electron mobility and conclude only that the electron mobility has not been substantially influenced by thiol treatment—but it is clear that it is not, within experimental error, increased.

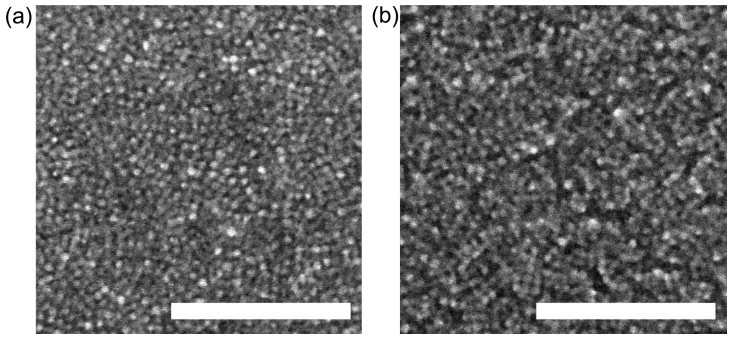

Figure 2. SEM images of PbS nanocrystal films treated with (a) 0.01% and (b) 0.05% ethanethiol, showing the formation of nanocracks in the overtreated film. The scale bar (bottom right) is 100 nm.

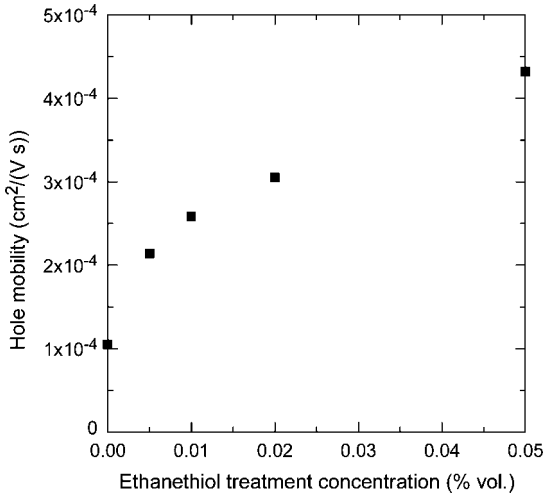

Figure 3. Hole mobility in PbS films as a function of ethanethiol treatment concentration.

Evaluation of Depletion Region Deepening Due to Thiol Treatments. In addition to its dependence on carrier transport, Schottky PV device performance is affected by changes in the depletion width and built-in potential (V_{bi}). We sought to investigate whether thiol treatments widened the depletion region, resulting in a larger drift-enabled collection volume. For this study, we employed capacitance−voltage ($C-V$) measurements.[23] From such measurements, we found that ethanethiol treatment resulted in a 30% decrease in zero-bias capacitance and an 80% increase in V_{bi}. The parameters extracted from these measurements, together with the corresponding PV performance parameters, are shown in Table 1. Using these zero-bias capacitance values, together with the static permittivity extracted from CELIV measurements, we estimated the depletion widths in the control and ethanethiol-treated devices to be 140 and 200 nm, respectively.

This increase in the depletion width of the device is consistent with a reduction in trap state density, as the presence of a large number of traps is known to affect the amount of band bending that occurs within the semiconductor bulk (rather than (undesirably) at the metal−semiconductor interface). Figure 4 is a schematic diagram of the energy levels in a Schottky diode device with and without a large density of surface states in the semiconductor. Figure 4a depicts the band bending in a control device, where a large density of interface traps limits the band bending in the bulk, while Figure 4b shows the greater degree of band bending

TABLE 1. Effect of Ethanethiol Treatment on Device Performance, Capacitance (C_0), Built-in Voltage (V_{bi}), and Acceptor Density (N_A)

	EQE (%)	V_{oc} (V)	C_0 (nF)	V_{bi} (V)	N_A ($\times 10^{16}$)
control	2.4	0.24	3.5	0.25	1.9
0.005%	6.4	0.36	2.6	0.46	2.5
0.01%	16.1	0.43	2.5	0.45	2.1

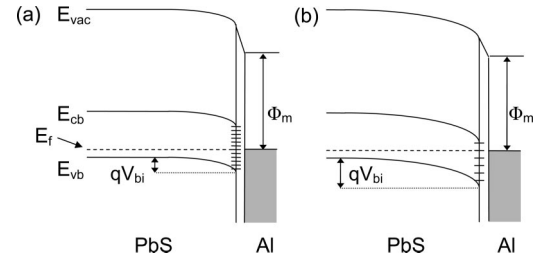

Figure 4. Schematic diagram showing the reduced band bending in a device with many interfacial traps (a) relative to one with fewer traps (b). Symbols denote the vacuum level (E_{vac}), conduction band (E_{cb}), Fermi level (E_f), valence band (E_{vb}), metal work function (Φ_m), and total band bending (qV_{bi}).

expected in a device where a significant number of these surface states have been passivated (*e.g.*, by ethanethiol).

Investigation of Impact of Thiols on Carrier Lifetime. Carrier lifetime also directly impacts device performance by improving both the drift length in the depletion region and the diffusion length in the quasi-neutral region.[8] V_{oc} decay measurements were obtained in order to estimate the lifetime of carriers under operating conditions. A transient 975 nm light pulse with an "on" intensity of 76 mW/cm^2 was used to excite the sample. The pulse width was chosen so that the voltage in the device saturated within the first 10% of the pulse's temporal width, ensuring that steady-state had been reached well prior to pulse turn-off and V_{oc} decay evaluation. Under these conditions, the carrier concentration at the instant the illumination is switched off should correspond to the carrier concentration in an operating device at open-circuit conditions, and the initial decay lifetime of the measured voltage should correspond to the carrier lifetime. Figure 5 shows the V_{oc} transients measured using this technique for a control device and an ethanethiol-treated device. The initial decay behavior is similar for both devices, but the control de-

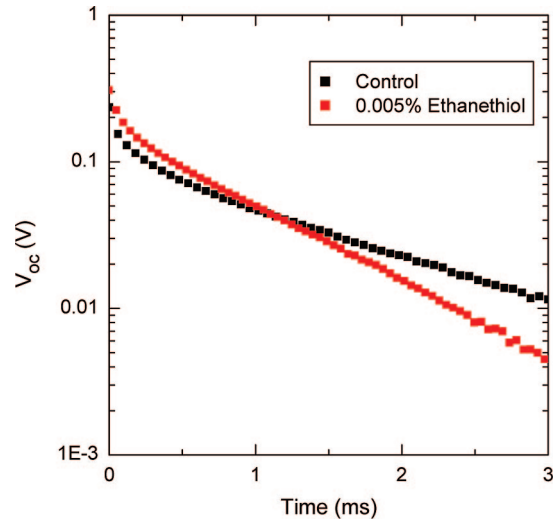

Figure 5. Open-circuit voltage decay following a 76 mW/cm^2 light pulse showing the long-lived tail in untreated control devices, indicative of increased trapping.

TABLE 2. Calculated Drift Length, Diffusion Length, and Depletion Width for Control Devices and Ethanethiol-Treated PV Devices

	control	ethanethiol-treated
drift length, electrons	3.8 μm	1.5 μm
drift length, holes	2.1 μm	6.3 μm
diffusion length	240 nm	140 nm
depletion width	140 nm	200 nm

vice exhibits a much longer lived tail than the ethanethiol-treated device. This long-lived component is believed to be a signature of trapped charges in the control device, which require more time to migrate by (activated) hopping in order to recombine.

Effect of Charge Extraction Enhancement on PV Performance. We now evaluate, within a simple physical model of device operation,[8] the extent to which the observed 4-fold improvement in EQE may be ascribed to each of three potential mechanisms:

Increased Drift-Transported Collection Volume Resulting from a Deepening of the Depletion Region. Table 2 shows the increase in depletion region thickness. Approximating the absorption profile throughout the device as uniform (which would if anything overestimate the role of collection from the depletion volume), the increased depletion region width accounts for at most a 1.4-fold increase in EQE. This upper limit assumes that there is no collection of carriers from the quasi-neutral region (QNR) of the device, so that the calculated 1.4-fold increase in depletion width is projected to produce a corresponding increase in EQE. In reality, there could be a significant contribution from the quasi-neutral region, as is the case in PbSe CQD devices,[13] which would reduce the impact of expanding the depletion region.

Increased Efficiency of Collection from the Depletion Region due to Increased Drift Length for One or Both Carriers. Included in Table 2 are the drift lengths for electrons and holes in control *versus* ethanethiol-treated devices. The drift lengths for electrons and holes (≥1.5 μm) both dramatically exceed the device thickness (≤250 nm). The observed changes in mobility and carrier lifetime are concluded to have little impact on efficiency of collection from the depletion region since this value is already near unity.

Increased Diffusion-Transported Collection Volume Resulting from an Increase in Electron Minority Carrier Diffusion Length. As seen in Table 2, the estimated electron minority carrier diffusion length is modestly decreased as a result of thiol treatments. Thus, in this study, thiols appear to provide no benefit to carrier collection from within the quasi-neutral region.

In sum, thiol-treatment-induced increases in carrier mobility and in depletion region depth account at most for a 50% improvement in EQE. These effects fail, on their own, to account for the observed 300% increase in EQE upon thiol treatment.

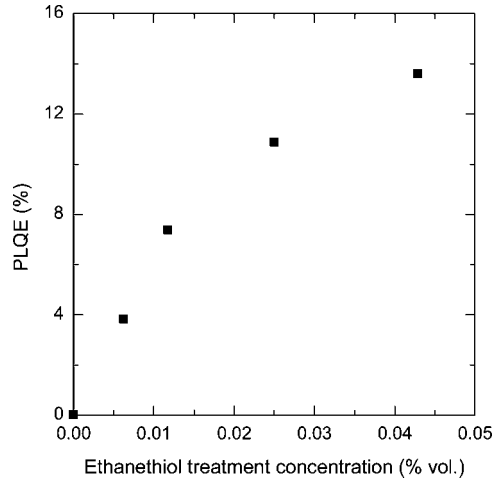

Figure 6. Photoluminescence quantum efficiency as a function of ethanethiol concentration in the nanocrystal solution.

Photoluminescence Studies. The photoluminescence behavior of quantum dots is known to depend strongly on the density and nature of surface states.[24−29] Since thiols are known to passivate surface states on many inorganic semiconductors,[30−33] we studied the luminescence from nanoparticles in octane solution as a function of ethanethiol concentration in an effort to elucidate the effects of ethanethiol on luminescence-quenching surface states. Figure 6 shows the solution-phase photoluminescence quantum efficiency (PLQE) as a function of ethanethiol concentration in the (octane) solution. It is apparent that the presence of ethanethiol has a dramatic impact on the PLQE, which increases from below the detection limit of our system (~0.5%) to more than 13%. We observed the same trend when treating nanocrystal films using thiols in the solid state, noting a 5-fold increase in thin-film PL brightness following optimum ethanethiol treatment. While the solution PLQE data suggest the form of an adsorption isotherm, higher thiol concentrations resulted in the nanocrystal's flocculation (possibly due to the removal of enough oleic acid ligands from the surface of the nanocrystals that the stability of the colloid is compromised), preventing the determination of an asymptotic limit to the PLQE.

Effect of Thiols on Exciton Dissociation Efficiency. The PLQE evidence both in solution and in the solid state point to a major added factor in the role of thiol treatments in PV device EQE: the efficiency of exciton dissociation must be increased by thiol treatment.

The EQE, $\eta_{external}$, of our device can be separated into three multiplicative components:[34]

$$\eta_{external} = \eta_{abs}\eta_{diss}\eta_{extr}$$

The absorption efficiency, η_{abs}, is simply the fraction of incident light absorbed by the device. The two remaining terms each correspond to a distinct time

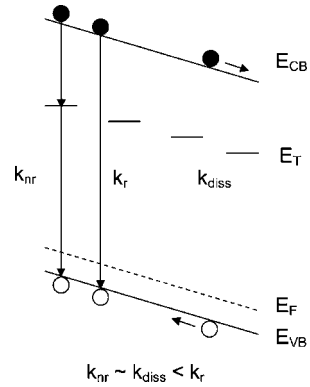

Figure 7. Schematic diagram showing one example of a nonradiative decay pathway, where a single deep trap level facilitates recombination between electrons in the conduction band and holes in the valence band. It is possible that the nonradiative decay occurs *via* a number of discrete trap levels in the band gap or even Auger recombination.

scale: η_{diss} represents the exciton dissociation quantum yield on the time scale of the radiative lifetime, typically in the 100 ns to microsecond regime for PbS[35] and PbSe[36] colloidal quantum dots. Thus, this term represents excited carriers' survival through the first hundreds of nanoseconds following their creation. The extraction efficiency, η_{extr}, quantifies the efficiency with which dissociated carriers are transported, through drift and diffusion, to their extracting contacts. We have found that these transport processes of dissociated (possibly shallow-trapped) carriers appear to occur more on time scales of many microseconds and greater.

As η_{abs} is unaffected by thiol treatment, and η_{extr} is increased at most 1.4-fold by thiol treatment; the increase in external quantum efficiency must arise from a considerable increase in η_{diss}.

The increase in η_{diss} is supported by the observed increase in PLQE, as the two phenomena are determined by many of the same processes. In the solid state, the dissocation efficiency is affected by the dissociation rate (k_{diss}) as well as the rate of competing radiative (k_r) and nonradiative recombination (k_{nr}) processes (Figure 7):

$$\eta_{diss} = \frac{k_{diss}}{k_{diss} + k_r + k_{nr}}$$

while in the solution, the PLQE, η_{PL}, is determined only by the relative radiative and nonradiative rates:

$$\eta_{PL} = \frac{k_r}{k_r + k_{nr}}$$

The increased PLQE in solution and in the solid state after thiol treatment suggests that the nonradiative recombination channels are being suppressed, and the reduction in the nonradiative rate is on the order of the PLQE increase (≥10). This reduction in k_{nr} leads to an increase in the dissociation efficiency and to the otherwise unanticipated increase in external quantum efficiency. The observed EQE increase can thus be associated with a roughly 3-fold increase in the dissociation efficiency, with the remaining, smaller, increase ascribed to extraction efficiency. Within the context of a recombination model as presented in the Shockley−Read−Hall model,[37] the nonradiative recombination rate in the bulk is proportional to the mid-gap trap state density, and as such, the increase in PLQE and exciton dissociation is also in agreement with the increased V_{oc}.

CONCLUSION

We have identified herein a major missing piece in the physical origins of high performance in colloidal quantum dot photovoltaic devices. The search for this missing piece was motivated by the failure of (modest) changes in measured carrier extraction alone to account for (major) improvements in EQE resulting from thiol treatments. We have proposed that the internal quantum efficiency of a PV device sees major influence on two time scales: one representing the competition between rapid, and undesired, trapping to mid-gap recombination centers; and the other representing the slower time scale competition between carrier extraction and carrier recombination from shallow traps.

METHODS

Chemicals. Lead(II) powder (PbO, 99%), oleic acid (OA, technical grade 90%), hexamethydisilathiane (TMS), 1-octadecene (ODE, technical grade 90%), toluene (anhydrous), methanol (anhydrous), isopropanol (anhydrous), and ethyl acetate were purchased from Sigma-Aldrich and used as received. Butylamine was purchased from Sigma-Aldrich and distilled prior to use.

Nanocrystal Synthesis and Isolation. The synthesis of PbS nanocrystals with an excitonic peak between 1500 and 1650 nm was performed using the standard air-free Schlenk-line technique. A stock solution of lead oleate (SS) was prepared by pumping the mixture of 4.0 mmol of PbO (0.9 g) and 63.0 mmol of OA (17.8 g) at 80 °C within 16 h. The sulfur precursor was made by mixing 2.0 mmol TMS with 10 mL of ODE in a nitrogen-filled glovebox. Twenty milliliters of SS was stirred vigorously while being heated to 150 °C under argon in a three-neck flask equipped with a condenser and thermocouple. The sulfur precursor was swiftly injected into the flask. The solution turned brown immediately after injection. The reaction was quenched by applying an ice−water bath. To isolate the nanocrystals, a mixture of 5 mL of anhydrous methanol and 5 mL of anhydrous ethyl acetate was injected into the flask and the dispersion centrifuged. After removing the supernatant, the mixture was re-dispersed in toluene and re-precipitated with methanol. The final PbS nanocrystals, with an average diameter of ~6 nm, were re-dispersed in toluene.

Butylamine Ligand Exchange. Nanocrystal ligand exchanges were performed in a N_2 glovebox (<20 ppm O_2). One milliliter of oleic-acid-capped nanocrystals was dispensed into a 15 mL test tube. One milliliter of butylamine was added and the solution mixed with a pipet. After ~1 min, the nanocrystals were precipitated by adding 12 mL of methanol. The nanocrystals were recovered by centrifuging for 1 min, pouring off the supernatant, and drying

under vacuum for 5 min. Butylamine was added to the dried nanocrystals to give a solution concentration of 100 mg/mL, and the solution was mixed vigorously until the nanocrystals had completely re-dispersed (~5 min). The nanocrystals were then precipitated with 12 mL of isopropanol, centrifuged 1 min, the supernatant decanted, and the remaining nanocrystals dried under vacuum again (5 min). The dried nanocrystals were completely dispersed to 100 mg/mL in butylamine again, and then precipitated with minimal isopropanol (approximately a 1:1 ratio by volume). After centrifuging, the lightly colored supernatant was poured off and the nanocrystals were dried by hand pumping 50 times with a pipet and large bulb. The dried nanocrystals were then dispersed in octane to 150 mg/mL. FTIR spectra of films of unexchanged and exchanged nanocrystals (Figure S2 in the Supporting Information) indicated that only ~40% of the oleic acid ligands were removed during the exchange.

Schottky PV Device Preparation. Commercial ITO-coated glass (Delta Technologies, 100 Ω, 1 in. × 1 in. squares) substrates were cleaned prior to film deposition by sonicating 30 min each in a 1% Triton-X/deionized (DI) water solution, isopropanol, and DI water. Cleaned substrates were then dried under a stream of N_2 and placed in a vacuum antechamber for 30 min to be loaded into a N_2 glovebox (<5 ppm O_2). Butylamine-exchanged nanocrystal solutions (150 mg/mL in octane) were spun onto the substrates at 500 rpm for 60 s. The resulting films were 230 ± 20 nm thick as measured by a Dektak profilometer. Samples were removed to air briefly before loading into an Edwards 306 evaporator and pumped down to a pressure of 1×10^{-5} Torr; 150 nm of Al was deposited followed by 150 nm of Ag, both at a rate of 0.5nm/s. A shadow mask was used to define a 4 × 4 array of 2 mm diameter circular contacts.

Ethanethiol Treatment of Nanocrystal Films. Films were treated in air immediately after spin-coating, prior to top contact deposition. The as-spun films were removed from the glovebox and placed in a covered Petri dish. Four hundred microliters of an ethanethiol/acetonitrile solution was pipetted onto the sample surface, making sure to cover the entire film. After 30 s, the treatment solution was poured off and the sample dried under a N_2 stream. Top contacts were then deposited as described above.

Device Characterization. *I*−*V* measurements were performed using a Keithley 2400 sourcemeter. *I*−*V* sweeps were generally performed between −1 and +1 V, with a step size of 0.02 V and a wait time of 100 ms at each point. Devices were illuminated from the ITO side, through a circular aperture with 2.5 mm diameter, using a 975 nm laser diode from QPhotonics. The output of the laser was fixed, and the illumination power was varied by using neutral density filters. *C*−*V* measurements were performed using an Agilent 4284A precision LCR meter. All measurements were performed in the dark in a shielded and grounded enclosure. For CELIV measurements, an Agilent 33120A function generator was used to generate a linearly increasing voltage pulse with an amplitude of 4 V and a rise time of 10 μs. The carrier extraction profiles were measured across a 50 Ω load with a Tektronix TDS220 digital oscilloscope. For V_{oc} transient measurements, devices were illuminated with a square wave light pulse generated by driving a QPhotonics 975 nm laser diode with an Agilent 33220A function generator. The light pulse duration (3 ms) was chosen such that the devices reached their V_{oc} value (as determined from their *I*−*V* curves) during the first 10% of the light pulse, to ensure the steady state had been reached before the pulse was switched off. V_{oc} decay transients were recorded on a Tektronix TDS 5104 digital oscilloscope with a 1 MΩ input impedance. For TOF mobility studies, devices with thick nanocrystal layers were made by placing several drops of nanocrystal solution onto the ITO substrate and waiting 30−60 s for some of the solvent to evaporate prior to spinning. These thick devices (>1.3 μm) were excited through the ITO contact using a yttrium−aluminum−garnet (YAG) laser operating at 532 nm with a 400 ns pulse width and 1 kHz repetition rate. The devices were biased with a Keithley 2400 sourcemeter, and a Tektronix TDS 5104 digital oscilloscope was used to measure the current transient output across a 50 Ω load.

Photoluminescence Quantum Efficiency Following Ethanethiol Treatment. A 10 mg/mL solution of PbS nanocrystals in octane was prepared and 300 μL placed into each of two cuvettes. The PLQE of each was measured, and then a known volume of ethanethiol/octane was added to one cuvette while an identical volume of octane was added to the other as a control before measuring the PLQE of each again. This procedure was repeated until the ethanethiol concentration passed a critical point at which the nanocrystals aggregate and no longer remain in solution.

Acknowledgment. The authors would like to thank J. Clifford for help with CELIV, *C*−*V*, and PL experiments, V. Sukhovatkin for help with time-of-flight measurements, and S. Myrskog for help with the PLQE setup. We would also like to thank E. Klem, G. Koleilat, G. Konstantatos, and S. Hinds for valuable discussions. A.R.B. acknowledges the financial support of the Natural Sciences and Engineering Research Council of Canada.

Supporting Information Available: FTIR data showing the extent of oleic acid removal by ethanethiol, FTIR data on as-synthesized (oleic acid capped) and butylamine-exchanged nanocrystals. This material is available free of charge *via* the Internet at http://pubs.acs.org.

REFERENCES AND NOTES

1. Mayer, A. C.; Scully, S. R.; Hardin, B. E.; Rowell, M. W.; McGehee, M. D. Polymer-Based Solar Cells. *Mater. Today* **2007**, *10*, 28–33.
2. Gur, I.; Fromer, N. A.; Geier, M. L.; Alivisatos, A. P. Air-Stable All-Inorganic Nanocrystal Solar Cells Processed from Solution. *Science* **2005**, *310*, 462–465.
3. Kim, J. Y.; Lee, K.; Coates, N. E.; Moses, D.; Nguyen, T. Q.; Dante, M.; Heeger, A. J. Efficient Tandem Polymer Solar Cells Fabricated by All-Solution Processing. *Science* **2007**, *317*, 222–225.
4. Zhang, J.; Jiang, X. M. Steady State Photoinduced Absorption of PbS Quantum Dots Film. *Appl. Phys. Lett.* **2008**, *92*, 141108-1–141108-3.
5. Fritz, K. P.; Guenes, S.; Luther, J.; Kumar, S.; Saricifitci, N. S.; Scholes, G. D. IV−VI Nanocrystal-Polymer Solar Cells. *J. Photochem. Photobiol. A* **2008**, *195*, 39–46.
6. Biancardo, M.; Krebs, F. C. Microstructured Extremely Thin Absorber Solar Cells. *Sol. Energy Mater. Sol. Cells* **2007**, *91*, 1755–1762.
7. Dissanayake, D.; Hatton, R. A.; Lutz, T.; Giusca, C. E.; Curry, R. J.; Silva, S. R. P. A PbS Nanocrystal-C-60 Photovoltaic Device for Infrared Light Harvesting. *Appl. Phys. Lett.* **2007**, *91*, 133506-1–133506-3.
8. Johnston, K. W.; Pattantyus-Abraham, A. G.; Clifford, J. P.; Myrskog, S. H.; Hoogland, S.; Shukla, H.; Klem, J. D.; Levina, L.; Sargent, E. H. Efficient Schottky-Quantum-Dot Photovoltaics: The Roles of Depletion, Drift, and Diffusion. *Appl. Phys. Lett.* **2008**, *92*, 122111-1–122111-3.
9. Johnston, K. W.; Pattantyus-Abraham, A. G.; Clifford, J. P.; Myrskog, S. H.; MacNeil, D. D.; Levina, L.; Sargent, E. H. Schottky-Quantum Dot Photovoltaics for Efficient Infrared Power Conversion. *Appl. Phys. Lett.* **2008**, *92*, 151115-1–151115-3.
10. Klem, E. J. D.; MacNeil, D. D.; Cyr, P. W.; Levina, L.; Sargenta, E. H. Efficient Solution-Processed Infrared Photovoltaic Cells: Planarized All-Inorganic Bulk Heterojunction Devices *via* Inter-Quantum-Dot Bridging During Growth from Solution. *Appl. Phys. Lett.* **2007**, *90*, 183113-1–183113-3.
11. Klem, E. J. D.; Shukla, H.; Hinds, S.; MacNeil, D. D.; Levina, L.; Sargent, E. H. Impact of Dithiol Treatment and Air Annealing on the Conductivity, Mobility, and Hole Density in PbS Colloidal Quantum Dot Solids. *Appl. Phys. Lett.* **2008**, *92*, 212105-1–212105-3.
12. Watt, A. A. R.; Blake, D.; Warner, J. H.; Thomsen, E. A.; Tavenner, E. L.; Rubinsztein-Dunlop, H.; Meredith, P. Lead Sulfide Nanocrystal: Conducting Polymer Solar Cells. *J. Phys. D: Appl. Phys.* **2005**, *38*, 2006–2012.
13. Koleilat, G. I.; Levina, L.; Shukla, H.; Myrskog, S. H.; Hinds, S.; Pattantyus-Abraham, A. G.; Sargent, E. H. Efficient, Stable Infrared Photovoltaics Based on Solution-Cast Colloidal Quantum Dots. *ACS Nano* **2008**, *2*, 833–840.

14. Law, M.; Luther, J. M.; Song, O.; Hughes, B. K.; Perkins, C. L.; Nozik, A. J. Structural, Optical, and Electrical Properties of PbSe Nanocrystal Solids Treated Thermally or with Simple Amines. *J. Am. Chem. Soc.* **2008**, *130*, 5974–5985.
15. Luther, J. M.; Law, M.; Song, Q.; Perkins, C. L.; Beard, M. C.; Nozik, A. J. Structural, Optical and Electrical Properties of Self-Assembled Films of PbSe Nanocrystals Treated with 1,2-Ethanedithiol. *ACS Nano* **2008**, *2*, 271–280.
16. Boettcher, S. W.; Strandwitz, N. C.; Schierhorn, M.; Lock, N.; Lonergan, M. C.; Stucky, G. D. Tunable Electronic Interfaces between Bulk Semiconductors and Ligand-Stabilized Nanoparticle Assemblies. *Nat. Mater.* **2007**, *6*, 592–596.
17. Sargent, E. H. Infrared Quantum Dots. *Adv. Mater.* **2005**, *17*, 515–522.
18. Konstantatos, G.; Clifford, J.; Levina, L.; Sargent, E. H. Sensitive Solution-Processed Visible-Wavelength Photodetectors. *Nat. Photonics* **2007**, *1*, 531–534.
19. Konstantatos, G.; Howard, I.; Fischer, A.; Hoogland, S.; Clifford, J.; Klem, E.; Levina, L.; Sargent, E. H. Ultrasensitive Solution-Cast Quantum Dot Photodetectors. *Nature* **2006**, *442*, 180–183.
20. Konstantatos, G.; Levina, L.; Fischer, A.; Sargent, E. H. Engineering the Temporal Response of Photoconductive Photodetectors *via* Selective Introduction of Surface Trap States. *Nano Lett.* **2008**, *8*, 1446–1450.
21. Hinds, S.; Levina, L.; Klem, E. J. D.; Konstantatos, G.; Sukhovatkin, V.; Sargent, E. H. Smooth-Morphology ($<$ 1% Roughness) Ultrasensitive Solution-Processed Visible Photodetectors. *Adv. Mater.*, **2008**, 10.1002/adma.200800452.
22. Juska, G.; Arlauskas, K.; Viliunas, M.; Kocka, J. Extraction Current Transients: New Method of Study of Charge Transport in Microcrystalline Silicon. *Phys. Rev. Lett.* **2000**, *84*, 4946–4949.
23. Clifford, J. P.; Johnston, K. W.; Levina, L.; Sargent, E. H. Schottky Barriers to Colloidal Quantum Dot Films. *Appl. Phys. Lett.* **2007**, *91*, 253117-1–253117-3.
24. Breus, V. V.; Heyes, C. D.; Nienhaus, G. U. Quenching of CdSe−ZnS Core−Shell Quantum Dot Luminescence by Water-Soluble Thiolated Ligands. *J. Phys. Chem. C* **2007**, *111*, 18589–18594.
25. Celebi, S.; Erdamar, A. K.; Sennaroglu, A.; Kurt, A.; Acar, H. Y. Synthesis and Characterization of Poly(Acrylic Acid) Stabilized Cadmium Sulfide Quantum Dots. *J. Phys. Chem. B* **2007**, *111*, 12668–12675.
26. Hammer, N. I.; Early, K. T.; Sill, K.; Odoi, M. Y.; Emrick, T.; Barnes, M. D. Coverage-Mediated Suppression of Blinking in Solid State Quantum Dot Conjugated Organic Composite Nanostructures. *J. Phys. Chem. B* **2006**, *110*, 14167–14171.
27. Javier, A.; Strouse, G. F. Activated and Intermittent Photoluminescence in Thin CdSe Quantum Dot Films. *Chem. Phys. Lett.* **2004**, *391*, 60–63.
28. Kippeny, T. C.; Bowers, M. J.; Dukes, A. D.; McBride, J. R.; Orndorff, R. L.; Garrett, M. D.; Rosenthal, S. J. Effects of Surface Passivation on the Exciton Dynamics of CdSe Nanocrystals as Observed by Ultrafast Fluorescence Upconversion Spectroscopy. *J. Chem. Phys.* **2008**, *128*, 084713-1–084713-7.
29. Fernee, M. J.; Watt, A.; Warner, J.; Cooper, S.; Heckenberg, N.; Rubinsztein-Dunlop, H. Inorganic Surface Passivation of PbS Nanocrystals Resulting in Strong Photoluminescent Emission. *Nanotechnology* **2003**, *14*, 991–997.
30. Remashan, K.; Bhat, K. N. Effects of Octa Decyl Thiol (ODT) Treatment on the Gallium Arsenide Surface and Interface State Density. *Thin Solid Films* **1999**, *342*, 20–29.
31. Lunt, S. R.; Ryba, G. N.; Santangelo, P. G.; Lewis, N. S. Chemical Studies of the Passivation of GaAs Surface Recombination Using Sulfides and Thiols. *J. Appl. Phys.* **1991**, *70*, 7449–7465.
32. Wuister, S. F.; Donega, C. D.; Meijerink, A. Influence of Thiol Capping on the Exciton Luminescence and Decay Kinetics of CdTe and CdSe Quantum. *J. Phys. Chem. B* **2004**, *108*, 17393–17397.
33. Tsuruoka, T.; Takahashi, R.; Nakamura, T.; Fujii, M.; Akamatsu, K.; Nawafune, H. Highly Luminescent Mono- and Multilayers of Immobilized CdTe Nanocrystals: Controlling Optical Properties through Post Chemical Surface Modification. *Chem. Commun.* **2008**, 1641–1643.
34. Hoppe, H.; Sariciftci, N. S. Organic Solar Cells: An Overview. *J. Mater. Res.* **2004**, *19*, 1924–1945.
35. Warner, J. H.; Thomsen, E.; Watt, A. R.; Heckenberg, N. R.; Rubinutein-Dunlop, H. Time-Resolved Photoluminescence Spectroscopy of Ligand-Capped PbS Nanocrystals. *Nanotechnology* **2005**, *16*, 175–179.
36. Wehrenberg, B. L.; Wang, C. J.; Guyot-Sionnest, P. Interband and Intraband Optical Studies of PbSe Colloidal Quantum Dots. *J. Phys. Chem. B* **2002**, *106*, 10634–10640.
37. Shockley, W.; Read, W. T. Statistics of the Recombinations of Holes and Electrons. *Phys. Rev.* **1952**, *87*, 835–842.